SCIENTIFIC REPORTS

OPEN

Magnetic field-dependent shape anisotropy in small patterned films studied using rotating magnetoresistance

Xiaolong Fan, Hengan Zhou, Jinwei Rao, Xiaobing Zhao, Jing Zhao, Fengzhen Zhang & Desheng Xue

Based on the electric rotating magnetoresistance method, the shape anisotropy of a Co microstrip has been systematically investigated. We find that the shape anisotropy is dependent not only on the shape itself, but also on the magnetization distribution controlled by an applied magnetic field. Together with micro-magnetic simulations, we present a visualized picture of how non-uniform magnetization affects the values and polarities of the anisotropy constants K_1 and K_2. From the perspective of potential appliantions, our results are useful in designing and understanding the performance of micro- and nano-scale patterned ferromagnetic units and the related device properties.

Shape anisotropy, which originates from the dipole-dipole interactions that occur in ferromagnets, is a fundamental issue in magnetism[1]. For uniformly magnetized magnetic ellipsoids bodies, the shape anisotropy can be quantificationally described by the demagnetization tensor **N** which depends only on the shape. Thus, it provides a simple mechanism for designing the local effective anisotropy field of micro- and nano-scale magnetic units[2–4]. However, for an arbitrary magnet with a non-ellipsoid shape (such as the commonly used square and rectangle), it is difficult to realize uniform magnetization under a finite magnetic field[5–7]. As a consequence of nonuniform magnetization, the values of **N** that are estimated by uniformly magnetized ellipsoid approximation would be inaccurate and not suitable for describing shape anisotropy[8,9]. Moreover, a magnetic field-dependent shape anisotropy is expected. As more and more micro- and nano-scale patterned ferromagnetic units are used in spintronics devices, the shape anisotropy plays an increasingly important role in determining both the magnetic properties of local magnets and the related device performances[10–14]. Therefore, it is time to systematically investigate the shape anisotropy in micro- and nano-scale magnetic units, which is important in both physics and applications.

Methods

The universal method for describing magnetic anisotropy is to determine the anisotropy constants K_i ($i = 1, 2, \ldots$) in the expression of magnetic anisotropy energy E_k. For uniaxial anisotropy, $E_k = K_1 \cos 2\theta + K_2 \cos 4\theta + \cdots$, where θ is the angle of the magnetization with respect to a certain symmetry axis. Many methods have been explored to measure magnetic anisotropy. Some methods can only give the first-order term K_1 or the effective anisotropy field H_k to estimate the anisotropy, such as the intersection method[15], the area method[16], and the singular point detection (SPD) method[17,18] but these methods are not sufficiently accurate for our experiments. There are also a few methods that can give higher-order terms, such as the torque method[19–21] and the magnetic resonance method[22,23]. It is worth noting that the ferromagnetic resonance (FMR) method is one of the best methods for

The Key Lab for Magnetism and Magnetic Materials of Ministry of Education, Lanzhou University, Tianshui South Road 222, 730000 Lanzhou, People's Republic of China. Correspondence and requests for materials should be addressed to X.F. (email: fanxiaolong@lzu.edu.cn)
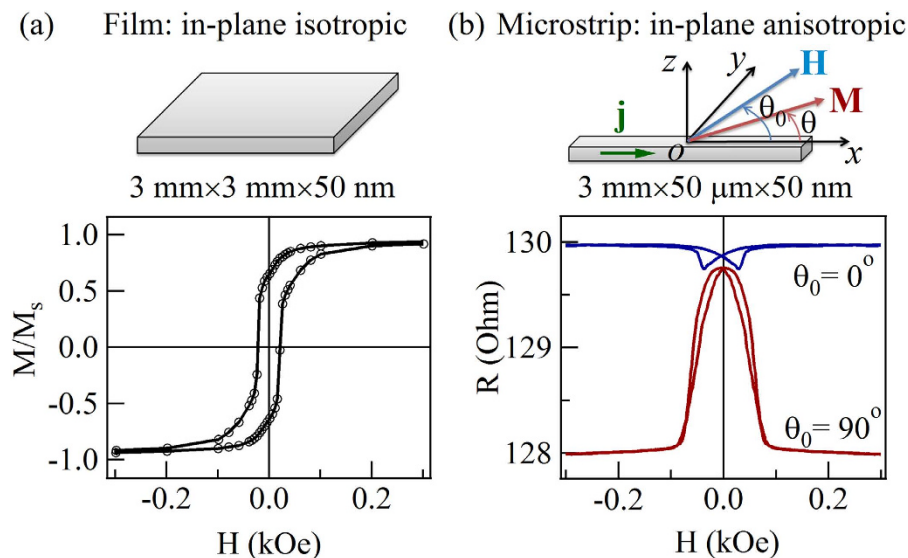
(a)   Film: in-plane isotropic   (b) Microstrip: in-plane anisotropic

Figure 1. The magnetic properties of the Co film and Co strip. (**a**) The magnetic hysteresis loop of Co film. (**b**) The magnetoresistance curves of a Co micro-strip at different θ_0.

determining magnetic anisotropy with very high sensitivity[24,25]. There are two kinds of FMR experiments, frequency-swept FMR and magnetic field-swept FMR. To obtain accurate anisotropy values, angular resolved measurements are needed, and K_i can be obtained by fitting the angle dependent resonance position curves ($H_r \sim \theta$ for field swept, $\omega_r \sim \theta$ for frequency swept). Such method can be realized using traditional cavity FMR, transmission line or co-planar waveguide[26–32], and DC electrical detection of FMR[33–44], and has been widely used in various magnetic materials. Note that, the field-swept FMR method is accurate only when the anisotropy itself is independent of the applied magnetic field, such as the magnetocrystalline anisotropy. If K_i is a function of the applied magnetic field (i.e., the shape anisotropy in our case), such a method becomes "inaccurate" because the relation between K_i and H_r is now hidden in $H_r \sim \theta$ and that relation cannot be directly obtained from the fitting. In this work, by taking the advantage of frequency-swept FMR and the torque method that determining anisotropy at a certain magnetic field, and the advantage of direct electrical detection which is its inherent high sensitivity, we used a similar but experimentally simpler DC electrical method to quantify the magnetic field-dependent shape anisotropy in a small magnetic unit.

Two samples were used in the experiments. One was a $3\,mm \times 3\,mm \times 50\,nm$ Co ferromagnetic film, and the other was a $3\,mm \times 50\,\mu m \times 50\,nm$ Co microstrip. Both samples were made of a Co film deposited on glass substrate using magnetron sputtering. The background pressure was lower than 6×10^{-5} Pa and a pressure of 0.2 MPa of argon was used. The patterns were realized using laser exposure and the lift-off method. The magnetoresistance was measured by using lock-in techniques: a lock-in amplifier (SR830) provided a 2 V voltage with a modulation frequency of 1.31 kHz, and the sample was connected with a large resistance (20 kΩ) in series. At the same time, the lock-in amplifier measured the voltage V_x at both ends of the microstrip. Thus, the resistance of the microstrip can be calculated using the expression $R = \frac{V_x}{2 + V_x} \times 20\,k\Omega$. The magnetic hysteresis loops were measured using a vibrating sample magnetometer (VSM; EV9, MicroSense, Westwood, MA, USA).

Results and Discussions

First, we measured the magnetic hysteresis loops of Co film with in-plane applied magnetic field H along different directions. All of the in-plane hysteresis loops were the same as shown in Fig. 1(a), which indicated that the Co film is in-plane isotropic. The saturation magnetization $M_s = 16.5\,kOe$ and coercivity $H_c = 27.5\,Oe$. However, because of the very small volume of the microstrip (approximately $7.5 \times 10^{-9}\,cm^3$), the maximal signal was approximately $9 \times 10^{-6}\,emu$, which is close to the resolution of the VSM. Then we used anisotropy magnetoresistance (AMR) curves (magnetoresistance as a function of magnetic field H) to identify the in-plane anisotropy of the microstrip, as shown in Fig. 1(b) where θ_0 is the angle of the applied magnetic field with respect to the long axis of the Co micro-strip. The significant differences between the curves show that the Co micro-strip is magnetic anisotropic. Comparing the results of Fig. 1(a) with Fig. 1(b), we can conform that the anisotropy of the Co microstrip originated from the shape anisotropy, and that the effective anisotropy field is approximately 80 Oe. Then, the problem becomes the following: how do we get the accurate value of anisotropy field? As noted in the method

section, the torque method can accurately measure anisotropy constants K_1 and K_2 by fitting the torque curve. Can the rotating anisotropy magnetorsistance (RAMR) $R_x \sim \theta_0$ curves give the accurate value of the shape anisotropy? Before we introduce the experiment results, comprehension of the features of the RAMR curve is necessary.

In the following, we calculate the RAMR curve at different magnetic field amplitudes by using the model shown in Fig. 1(b). The expression of AMR is given by[11]

$$R_x = R_0 + \Delta R \ \cos^2 \theta, \tag{1}$$

where, R_0 is ordinary resistance, ΔR is the anisotropy magnetoresistance, and θ is the orientation of magnetization M with respect to the current density j_x. Our first task is to determine θ from the equilibrium condition when applying a magnetic field with amplitude H and direction θ_0. Based on the coherent rotation model, the total energy is given by

$$E_{total} = K_1 \ \cos 2\theta + K_2 \ \cos 4\theta - \mu_0 M_s H \ \cos (\theta_0 - \theta). \tag{2}$$

The equilibrium direction of magnetization is determined by the minimum of E_{total} with respect to θ, i.e. $\partial E_{total} / \partial \theta = 0$ and $\partial^2 E_{total} / \partial \theta^2 > 0$,

$$2K_1 \ \sin 2\theta + 4K_2 \ \sin 4\theta + \mu_0 M_s H \ \sin (\theta_0 - \theta) = 0, \tag{3}$$

$$-4K_1 \ \cos 2\theta - 16K_2 \ \cos 4\theta + \mu_0 M_s H \ \cos(\theta_0 - \theta) > 0. \tag{4}$$

Considering $K_1 < 0$ (i.e., the easy axis lies along the x axis), the anisotropy field H_k and reduced magnetic field h_i ($i = 1, 2, 3\cdots$) can be defined as:

$$H_k^{(1)} = \frac{-4K_1}{\mu_0 M_s}, \ H_k^{(2)} = \frac{-16K_2}{\mu_0 M_s}, \ h_i = \frac{H}{H_k^{(i)}}. \tag{5}$$

If we ignore K_2 temporarily for a simple case, Eqs. (3) and (4) can be simplified as

$$\frac{1}{2} \ \sin 2\theta - h_1 \sin (\theta_0 - \theta) = 0, \tag{6}$$

$$\cos 2\theta + h_1 \cos (\theta_0 - \theta) > 0, \tag{7}$$

Based on Eqs. (6) and (7), we can calculate the relation of $\theta \sim \theta_0$ with any selected h_1 value. Putting $\theta \sim \theta_0$ into Eq. (1), the angular dependence of the magnetoresistance (i.e., the RAMR curve $R_x \sim \theta_0$) can be obtained. Supposing $R_0 = 100\,\Omega$, $\Delta R = 2\,\Omega$, the $R_x \sim \theta_0$ curves have been calculated at different h_1; as shown in Fig. 2. Those curves can be divided into three groups with quite different features. Group 1: $h_1 < 0.5$, as shown in Fig. 2(a,b), both the $\theta \sim \theta_0$ curves and $R_x \sim \theta_0$ curves are continuous, and have a period of $360°$, which indicates that the magnetization process is reversible under small applied magnetic fields. Group 2: $0.5 \leq h_1 \leq 1$; as shown in Fig. 2(c,d), the curves are obtained at relatively high applied fields. It is found that the periods of these curves are $180°$ rather than $360°$, and that two "jumps" appear, which makes the curves discontinuous. The "jumps" results from an irreversible rotation of magnetization from current state to a more steady equilibrium state at critical values of θ_0[45]. Group 3: $h_1 > 1$; as plotted in Fig. 2(e,f), although the period is $180°$, the curves become continuous again, which indicates that the magnetization is approaching the saturation state.

Immediately thereafter, we measured the RAMR curves of the Co micro-strip at different H, and the raw data (symbols) are shown in Fig. 3(a). The RAMR curve measured at $H = 34.3\,Oe$ has features similar to the second group's theoretical curves shown in Fig. 2(d), wherein two obvious "jumps" can be observed. The curves measured at $H = 126.0\,Oe$ and $303.0\,Oe$ look similar to those of the third group shown in Fig. 2(f). Therefore, our experimental results are basically consistent with the theory. We also measured the $R_x \sim \theta_0$ curve at $H = 22\,Oe$, which should be corresponding to the case of the first group. However, as the applied magnetic field is relative small, the magnetization switching mechanism is domain wall motion rather than coherent rotation as shown in supplementary material. Thus, the cases $h < 0.5$ are not suitable for determining the anisotropy constants, we did not add the cases $h < 0.5$ in this letter.

An accurate anisotropy field can be obtained by fitting the normalized torque curves $\sin (\theta_0 - \theta) \sim \theta$, as shown in Fig. 3(b). The angle θ was calculated from the RAMR curves by using Eq. (1) with $R_0 = 127.94\,\Omega$ and $\Delta R = 2.05\,\Omega$, as determined previously. The fitting function is a transformation of Eq. (3), given by
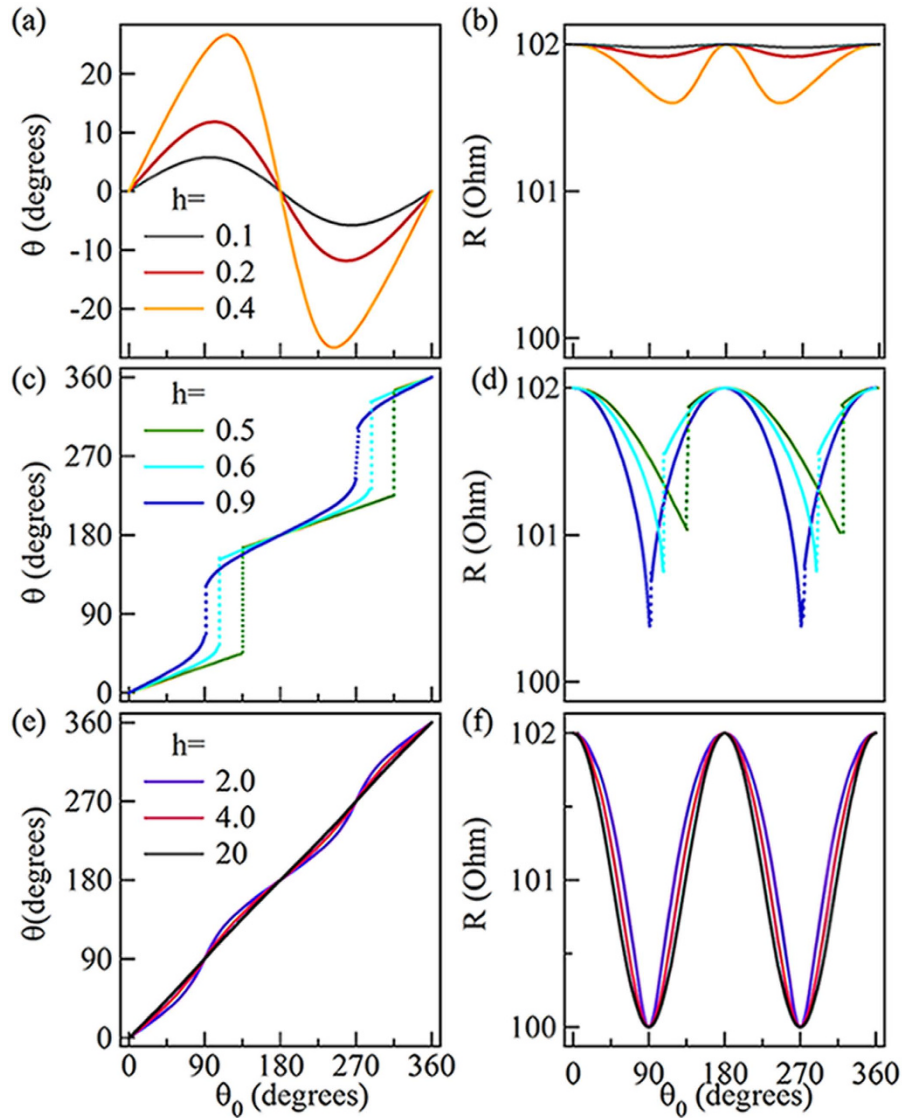
Figure 2. The calculated $\theta \sim \theta_0$ curves and RAMR curves. (**a,c,e**) The calculated $\theta \sim \theta_0$ curves at different h. (**b,d,f**) The magnetoresistance (R_x) as a function of θ_0 at different h.

$$\sin(\theta_0 - \theta) = \frac{1}{2}\frac{H_k^{(1)}}{H}\sin 2\theta + \frac{1}{4}\frac{H_k^{(2)}}{H}\sin 4\theta. \tag{8}$$

As shown in Fig. 3(b), the experimental results can be well fitted with that equation, which gives birth to the values of $H_k^{(1)}$ and $H_k^{(2)}$. Moreover, the anisotropy constants K_1 and K_2 can be calculated using Eq. (5), as shown in Table 1. However, the values of K_1 (K_2) shown in the table differ from one another. To verify whether those values are correct, we took the values of K_1, K_2 and H in the table back to Eq. (3) and (4), and then calculated the $R_x \sim \theta_0$ curves, i.e. the red curves shown in Fig. 3(a). The well matching between the experimental data and calculated curves indicates that all of the values shown in the table are correct. In the supplement, there is a discussion about the importance of higher-order terms in the fitting results, which is the circumstantial evidence of the accuracy of this method.

The difference between K_1 and K_2 determined under different H unveils a fundamental issue in magnetism: the shape anisotropy not only is determined by the shape itself, but also depends on the applied magnetic field. It has been written in every textbook of magnetism that the shape anisotropy of any non-ellipsoid magnet is a complicated issue because of the non-uniform magnetization. Therefore, it is not surprising that the shape anisotropy is field dependent. However, because the non-uniform magnetization cannot be quantified simply, theoretical calculations of shape anisotropy in non-ellipsoid magnets are quite complicated. Because accurate anisotropy constants can now be experimentally determined, we
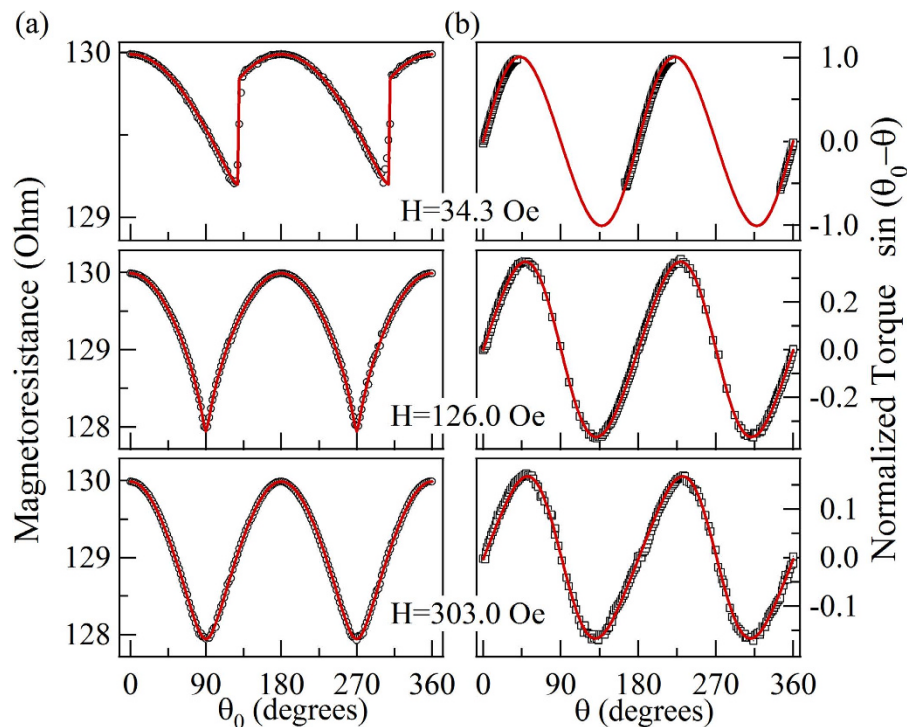
Figure 3. The RAMR curves and normalized torque curves obtained in different magnetic fields. (a) Symbols represent experimental $R_x \sim \theta_0$ curves measured at $H = 34.3\,\text{Oe}$, $126.0\,\text{Oe}$, and $303.0\,\text{Oe}$ respectively; red lines are calculated curves used for corresponding fitted anisotropy constants. **(b)** The data of normalized torque curves $\sin(\theta_0 - \theta)$ as a function of θ; symbols are experimental data and the solid curves are fitting curves based on Eq. (8).

H	H_k^1	H_k^2	K_1	K_2
(Oe)	(Oe)	(Oe)	(kerg/cm^3)	(kerg/cm^3)
34.3	68.8	7.3	-22.58	-0.60
126.0	92.0	-13.6	-30.20	1.12
303.0	99.0	-20.8	-32.50	1.71

Table 1. The magnetic anisotropy parameters measured at different H.

systematically measured the shape anisotropy constants at different H as shown in Fig. 4(a). It is found that when $H < 200\,\text{Oe}$, both the amplitudes of K_1 and K_2 vary obviously with H; when $H > 200\,\text{Oe}$, K_1 and K_2 are saturated. Those experimental results can be further supported by the simulated H dependent K_1 and K_2, as in the insert shown in Fig. 4(a). We calculated the angular dependent demagnetization energy curves and fitted them with $E_k = K_1 \cos 2\theta + K_2 \cos 4\theta$ to determine the values of K_1 and K_2. The OOMMF[46] was used to simulate the demagnetization energy of a Co strip. In the simulations, the Co strip had a length $a = 30\,\mu\text{m}$, and width $b = 0.5\,\mu\text{m}$, which has the same aspect ratio as our sample; the strip thickness was $d = 5\,\text{nm}$, and the unit cell size was $5 \times 5 \times 5\,\text{nm}^3$. Material parameters used were typical for Co, namely, saturation magnetization $M_s = 1.4 \times 10^6\,\text{Am}^{-1}$, and exchange stiffness constant $A = 3 \times 10^{-11}\,\text{Jm}^{-1}$[47]. As shown in Fig. 4(a), the simulative curves (inset) have the same tendency as the experimental curves, which indicates that the measured results of H-dependent K_1 and K_2 are reasonable.

To present a visualized picture of how the non-uniform magnetization affects the values and polarities of K_1 and K_2, the distributions of M in a squareness ratio $a/b = 60{:}1$ Co strip were simulated with applied magnetic field $H = 50\,\text{Oe}$, $400\,\text{Oe}$ and $1600\,\text{Oe}$, as shown in Fig. 4(c). The arrows represent the direction of M, and the color stands for the amplitude of the magnetic moment along the strip. Obviously, the non-uniformed magnetization emerges at the edge of the strip. With an increasing magnetic field, the magnetization distribution becomes uniform, which can be directly linked to the H-dependent K_1 and K_2. Therefore, for non-uniformly magnetized magnets, the shape anisotropy depends not only on
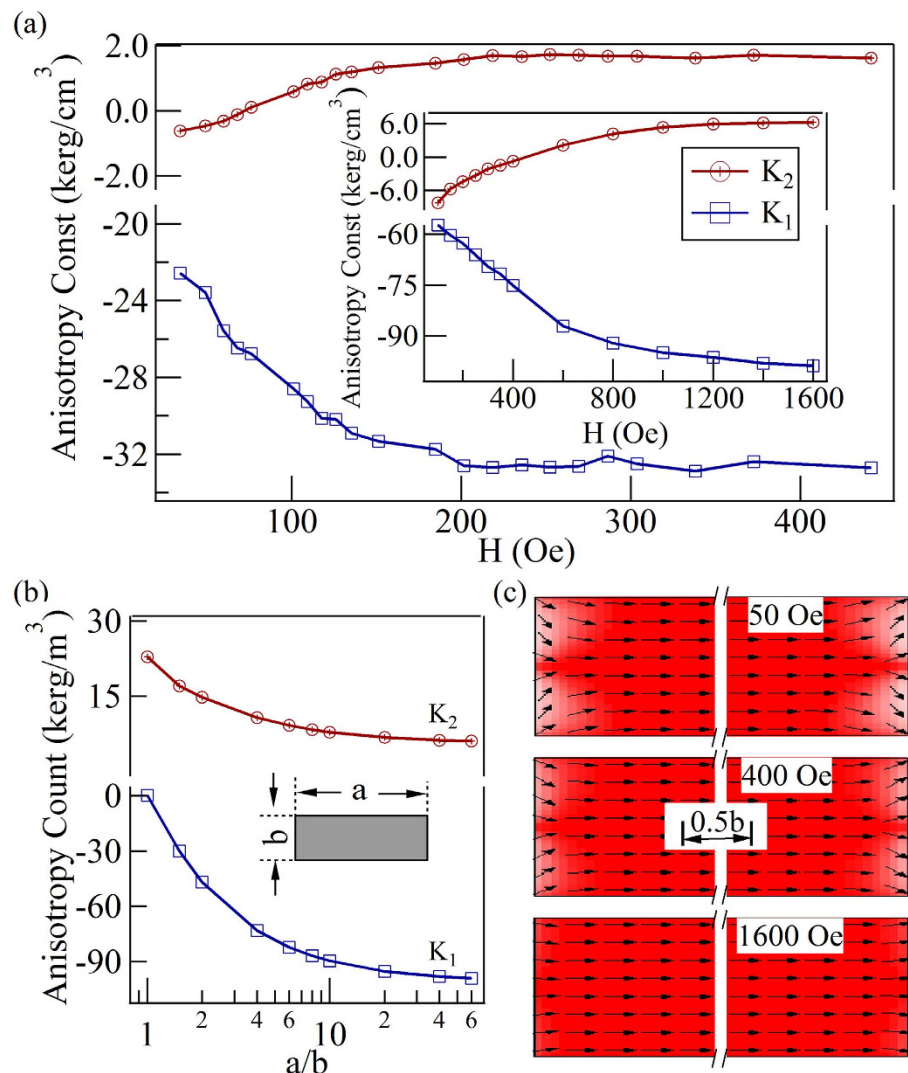
Figure 4. The magnetic field-and aspect ratio-dependent anisotropy constants. (a) The relationship between anisotropy constants and magnetic field; the insert is the simulative result. **(b)** The simulative K_1 and K_2 as a function of the rate of a:b. (c) The distribution of magnetic moments at different magnetic fields obtained by the micro-magnetic simulation.

the shape, but also on the magnetization distribution controlled by the applied magnetic field. In the following, we want to discuss the polarity of the anisotropy constants. Both the experimental and simulation results show that K_1 and K_2 have opposite polarity ($K_1 < 0$ and $K_2 > 0$) in the saturation status. The polarity actually represents the direction of the easy axis. To illustrate this argument, we simulated the values of K_1 and K_2 as functions of the squareness ratio with a sufficiently large applied magnetic field $H = 1600$ Oe as shown in Fig. 4(b). When the squareness ratio is 1:1, $K_1 = 0$, $K_2 > 0$, the anisotropy energy can be written as $E_K = K_2 \cos4\theta$, and the minimum of E_k appears at $\theta = (2n + 1)\pi/4$ i.e. the easy axis is along the cater-corner, which is consistent with the previously reported results[47]. When the squareness ratio $a/b > 1$, K_2 decreases slightly and K_1 appears with negative values. The amplitude of K_1 increases rapidly and becomes dominant, which means that the easy axis is along the strip.

We studied the influences of effective exchange stiffness constant A, saturation magnetization M_s, and film thickness d on the values of the shape anisotropy obtained at saturation magnetized condition using simulation. We changed one parameter for the simulation while the other parameters remained the same as the previous ones. As show in Fig. 5(a), the anisotropy constants did not vary significantly while A changed from 3×10^{-11} Jm^{-1} to 2×10^{-11} Jm^{-1}. As show in Fig. 5(b), while the M_s changed from 12.6 kOe (1.4×10^6 Am^{-1}) to 17.6 kOe (1×10^6 Am^{-1}), the amplitude of K_1 and K_2 increased almost linearly with M_s, which is the nature of demagnetization energy. Moreover, the simulations with the cases where $d = 3$ nm (cell sizes $= 3 \times 3 \times 3$ nm^3), 4 nm (cell sizes $= 4 \times 4 \times 4$ nm^3), 5 nm, 10 nm, 15 nm, and
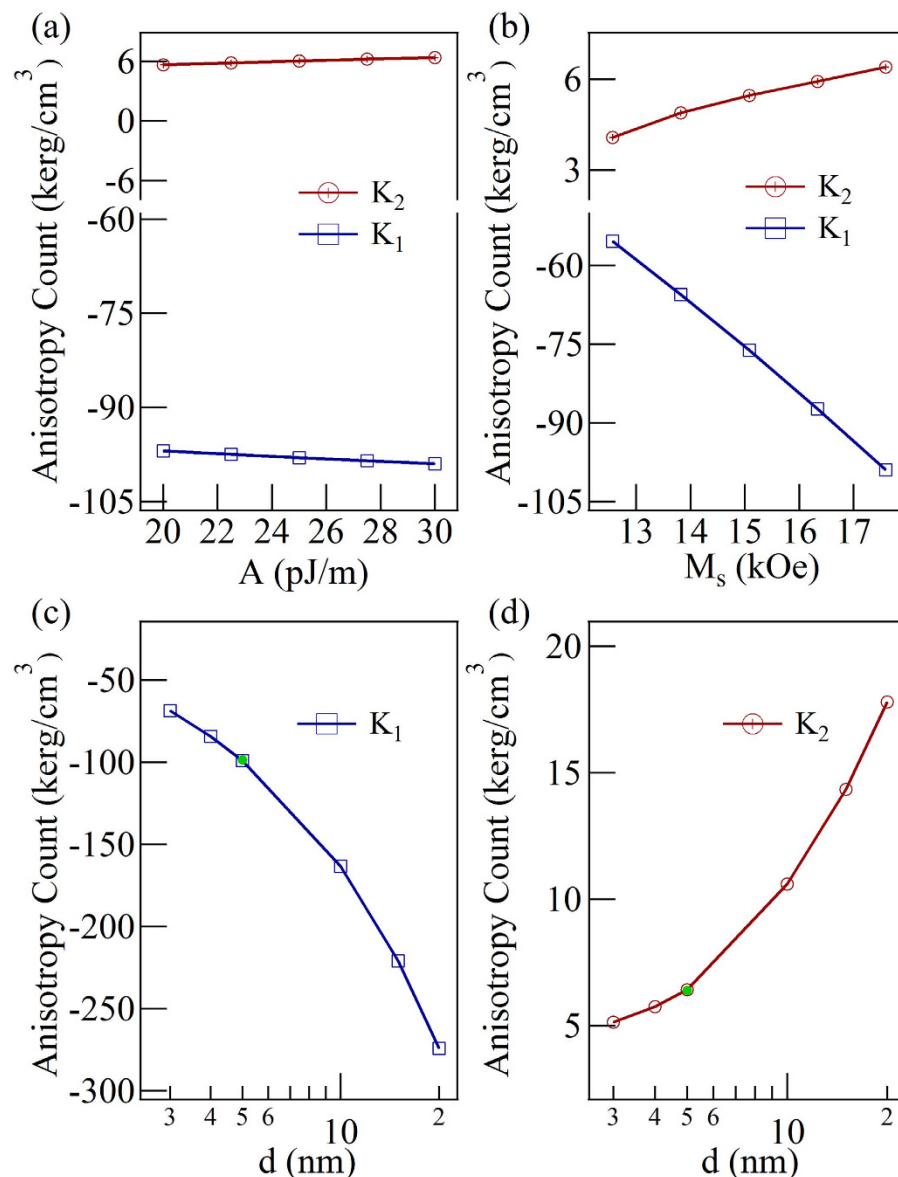
Figure 5. The simulated anisotropy constants change with the exchange stiffness constant, saturation magnetization and thickness. (**a**) The relationship between anisotropy constants and the amplitude of the exchange stiffness constant. (**b**) The simulated K_1 and K_2 as a function of the saturation magnetization. (**c**) The thickness dependent anisotropy constant K_1. (**d**) The thickness dependent anisotropy constant K_2.

20 nm (cell sizes $= 5 \times 5 \times 5$ nm^3) were performed, as shown in Fig. 5(c,d). Additionally, the green points represented the simulated results of $d = 5$ nm using smaller cell size $2.5 \times 2.5 \times 2.5$ nm^3, which is consistent with previous case. Therefore, the influence of the unit cell size on the simulation results can be ignored. It should be noted that the simulated values for K_1 (K_2) in Fig. 4(a) are different from the experimental ones, the main reason comes from the thickness we used for the simulations. The size of the experimental sample was 3 mm$\times 50$ μm $\times 50$ nm; to meet the proportion, the size of the simulated strip should be 30μm $\times 0.5 \mu$m $\times 0.5$ nm. However, if we use cell sizes $= 0.5 \times 0.5 \times 0.5$ nm^3, the simulation would be far beyond our calculation ability. According to the tendency shown in Fig. 5(c,d), the value of K_1 (K_2) may reach -35 kerg/cm^3 (2.2 kerg/cm^3) when $d = 0.5$ nm, which is close to the experimental values.

In fact, the shape anisotropy, which originates from the dipolar-dipolar interaction, is an old but fundamental problem in magnetism. The difficulty in calculating of shape anisotropy in non-ellipsoid magnets comes from the fact that non-uniform magnetization cannot be simply quantified. Because we can now quantify accurately the shape anisotropy which is closely related to the non-uniform magnetization, the magnetic field-dependent K_1 and K_2 determined by our method may be semi-quantificational

parameters for describing non-uniform magnetization. From the application perspective, both shape anisotropy and non-uniform magnetization are important in designing and understanding the performance of micro- and nano-scale patterned ferromagnetic units as well as the related device properties.

Conclusions

In conclusion, based on the RAMR method, the shape anisotropy of a Co micro-strip was systematically studied. It was found that using only demagnetization factor is not sufficient to describe the shape anisotropy of non-ellipsoid magnets, and that non-uniform magnetization would result in an H-dependent anisotropy. These results have also been demonstrated through micromagnetic simulations.

References

1. Holstein, T. & Primakoff, H. Field dependence of the intrinsic domain magnetization of a ferromagnet. *Phys. Rev.* **58,** 1098 (1940).
2. Pardavi-Horvath, M., Yan, J. & Peverley, J. R. Nonuniform internal field in planar ferrite elements. *IEEE Trans. Magn.* **37,** 3881 (2001).
3. Kobayashi, M. & Ishikawa, Y. Surface magnetic charge distributions and demagnetizing factors of circular cylinders. *IEEE Trans. Magn.* **28,** 1810 (1992).
4. Osborn, J. A. Demagnetizing factors of the general ellipsoid. *Phys. Rev.* **67,** 351 (1945).
5. Dubowik, J. Shape anisotropy of magnetic heterostructures. *Phys. Rev. B* **56,** 4088 (1996).
6. Jonsson, T., Nordblad, P. & Svedlindh, P. Dynamic study of dipole-dipole interaction effects in a magnetic nanoparticle system. *Phys. Rev. B* **57,** 497 (1998).
7. Li, Z. B., Zhang, M., Shen, B. G. & Sun, J. R. Non-uniform magnetization reversal in nanocomposite magnets. *Appl. Phys. Lett.* **102,** 102405 (2013).
8. Chen, D., Pardo, E. & Sanchez, A. Demagnetizing factors of rectangular prisms and ellipsoids. *IEEE Trans. Magn.* **38,** 1742 (2002).
9. Joseph, R. I. & Schlämann, E. Demagnetizing field in n onellipsoidal bodies. *J. Appl. Phys.* **36,** 5 (1965).
10. Fluitman, J. H. J. The influence of sample geometry on the magnetoresistance of ni-fe films. *Thin Solid Films* **16,** 269–276 (1973).
11. Kima, D. Y., Kimb, C. G., Parkb, B. S. & Parkc, C. M. Thickness dependence of planar hall resistance and field sensitivity in nio(30 nm)/nife(t) bilayers. *J. Magn. Magn. Mater.* **215–216,** 585–588 (2000).
12. Lu, Y. *et al.* Shape-anisotropy-controlled magnetoresistive response in magnetic tunnel junctions. *Appl. Phys. Lett.* **70,** 2610 (1997).
13. Kimura, T. & Wakaya, F. K. G. Control of magnetization rotation using submicron-wide cross geometry. *J. Magn. Magn. Mater.* **248,** 286–291 (2002).
14. Lin, M., Fan, X. L., Zhang, Z. M., Guo, D. W. & Xue, D. S. In-plane uniaxial anisotropy induced by two-phase stripelike magnetic hybrid structure. J. *Appl. Phys.* **106,** 123912 (2009).
15. Fayling, R. E. Relationship between coercive force and anisotropy field for oriented barium ferrite tapes and magnets. *J. Appl. Phys.* **49,** 1823 (1978).
16. Strnat, K., Hoffer, G., Olson, J., Ostertag, W. & Becker, J. J. A family of new cobalt-base permanent magnet materials. *J. Appl. Phys.* **38,** 1001 (1967).
17. Scholl, R., Elk, K. & Jahn, L. Application of the spd-method to crystalline and polycrystalline permanent magnetic materials. *J. Magn. Magn. Mater.* **82,** 1–3 (1989).
18. Nishioy, H. *et al.* A comparison of magnetic anisotropy constants and anisotropy fields of permanent magnets determined by various measuring methods. *J. Phys. D: Appl. Phys.* **29,** 2240 (1996).
19. Palmer, W. Magnetocrystalline anisotropy of magnetite at low temperature. *Phys. Rev.* **131,** 1057 (1963).
20. Aubert, G. Torque measurements of the anisotropy of energy and magnetization of nickel. *J. Appl. Phys.* **39,** 504 (1968).
21. Kouvel, J. S. & Graham, C. D. On the determination of magnetocrystalline anisotropy constants from torque measurements. *J. Appl. Phys.* **28,** 340 (1957).
22. Zhou, H. *et al.* Electric field controlled reversible magnetic anisotropy switching studied by spin rectification. *Appl. Phys. Lett.* **104,** 102401 (2014).
23. Fan, X. *et al.* Rapid characterizing of ferromagnetic materials using spin rectification. *Appl. Phys. Lett.* **105,** 262404 (2014).
24. Jalali-Roudsar, A. A., Denysenkov, V. P. & Khartsev, S. I. Determination of magnetic anisotropy constants for magnetic garnet epitaxial films using ferromagnetic resonance. *J. Magn. Magn. Mater.* **288,** 15–21 (2005).
25. Heinrich, B. & Cochran, J. Ultrathin metallic magnetic films: magnetic anisotropies and exchange interactions. *Adv. in Phys.* **42,** 15–21 (1993).
26. Kittel, C. On the theory of ferromagnetic resonance absorption. *Phys. Rev.* **73,** 155 (1948).
27. Chappert, C., Dang, K. L., Beauvillain, P., Hurdequint, H. & Renard, D. Ferromagnetic resonance studies of very thin cobalt films on a gold substrate. *Phys. Rev. B* **34,** 3192 (1986).
28. Farle, M. Ferromagnetic resonance of ultrathin metallic layers. *Rep. Prog. Phys.* **61,** 755 (1998).
29. Bickford, L. R. Ferromagnetic resonance absorption in magnetite single crystals. *Phys. Rev.* **78,** 449 (1950).
30. Heinrich, B. *et al.* Ferromagnetic-resonance study of ultrathin bcc fe(100) films grown epitaxially on fcc ag(100) substrates. *Phys. Rev. Lett.* **59,** 1756 (1987).
31. Liu, X., Sasaki, Y. & Furdyna, J. K. Ferromagnetic resonance in ga1-xmnxas: Effects of magnetic anisotropy. *Phys. Rev. B* **67,** 205204 (2003).
32. Schlämann, E., Green, J. J. & Milano, U. Recent developments in ferromagnetic resonance at high power levels. *J. Appl. Phys.* **31,** 386 (1960).
33. Costache, M. V., Watts, S. M., Sladkov, M., van der Wal, C. H. & van Wees, B. J. Large cone angle magnetization precession of an individual nanopatterned ferromagnet with dc electrical detection. *Appl. Phys. Lett* **89,** 232115 (2006).
34. Harder, M., Cao, Z. X., Gui, Y. S., Fan, X. L. & Hu, C.-M. Analysis of the line shape of electrically detected ferromagnetic resonance. *Phys. Rev. B* **84,** 054423 (2011).
35. Zhu, X. F. *et al.* Dielectric measurements via a phase-resolved spintronic technique. *Phys. Rev. B* **83,** 104407 (2011).
36. Gui, Y. S., Mecking, N., Zhou, X., Williams, G. & Hu, C. M. Realization of a room-temperature spin dynamo: The spin rectification effect. *Phys. Rev. Lett.* **98,** 107602 (2007).
37. Wirthmann, A. *et al.* Direct phase probing and mapping via spintronic michelson interferometry. *Phys. Rev. Lett.* **105,** 017202 (2010).
38. Gui, Y. S., Wirthmann, A. & Hu, C. C. Foldover ferromagnetic resonance and damping in permalloy microstrips. *Phys. Rev. B* **80,** 184422 (2009).

39. Gui, Y. S., Wirthmann, A., Mecking, N. & Hu, C.-M. Direct measurement of nonlinear ferromagnetic damping via the intrinsic foldover effect. *Phys. Rev. B* **80,** 060402 (2009).
40. Kiselev, S. I. *et al.* Microwave oscillations of a nanomagnet driven by a spin-polarized current. *Nature* **425,** 380 (2003).
41. Sankey, J. C. *et al.* Spin-transfer-driven ferromagnetic resonance of individual nanomagnets. *Phys. Rev. Lett.* **96,** 227601 (2006).
42. Sankey, J. C. *et al.* Measurement of the spin-transfer-torque vector in magnetic tunnel junctions. *Nat. Phys.* **4,** 67 (2008).
43. Liu, L., Moriyama, T., Ralph, D. C. & Buhrman, R. A. Spin-torque ferromagnetic resonance induced by the spin hall effect. *Phys. Rev. Lett.* **106,** 036601 (2011).
44. Sandweg, C. W., Kajiwara, Y., Ando, K., Saitoh, E. & Hillebrands, B. Enhancement of the spin pumping efficiency by spin wave mode selection. *Appl. Phys. Lett.* **97,** 252504 (2010).
45. Fan, X., Xue, D., Jiang, C., Gong, Y. & Li, J. An approach for researching uniaxial anisotropy magnet: Rotational magnetization. *J. Appl. Phys.* **102,** 123901 (2007).
46. Donahue, M. & Porter, D. Oommf user's guide, version 1.0. interagency report nistir 6376. *NIST* (1999).
47. Ren, Y. *et al.* Tailoring coercivity and magnetic anisotropy of co nanowire arrays by microstructure. *J. Mater. Sci.* **46,** 7545–7550 (2011).

Acknowledgements

Author Contributions

X.L.F. and H.A.Z. provide the idea and designed this study. H.A.Z. performed the experiments under the guidance of X.L.F. and D.S.X. J.W.R., X.B.Z., J.Z.H. and F.Z.Z. participated in the coordination of the study. D.S.X. and X.L.F. provide the fund support. All authors discussed the results. H.A.Z. and X.L.F. completed the manuscript. All authors read and approved the final manuscript.

Additional Information

Supplementary information accompanies this paper at http://www.nature.com/srep

Competing financial interests: The authors declare no competing financial interests.

How to cite this article: Fan, X. *et al.* Magnetic field-dependent shape anisotropy in small patterned films studied using rotating magnetoresistance. *Sci. Rep.* **5**, 16139; doi: 10.1038/srep16139 (2015).